



LAWRENCE
LIVERMORE
NATIONAL
LABORATORY

Density functional theory calculations of magnetocrystalline anisotropy energies for $(\text{Fe}_{1-x}\text{Co}_x)_2\text{B}$

M. Daene, S. K. Kim, M. P. Surh, D. Aberg, L. X. Benedict

March 12, 2015

Journal of Physics: Condensed Matter

Disclaimer

This document was prepared as an account of work sponsored by an agency of the United States government. Neither the United States government nor Lawrence Livermore National Security, LLC, nor any of their employees makes any warranty, expressed or implied, or assumes any legal liability or responsibility for the accuracy, completeness, or usefulness of any information, apparatus, product, or process disclosed, or represents that its use would not infringe privately owned rights. Reference herein to any specific commercial product, process, or service by trade name, trademark, manufacturer, or otherwise does not necessarily constitute or imply its endorsement, recommendation, or favoring by the United States government or Lawrence Livermore National Security, LLC. The views and opinions of authors expressed herein do not necessarily state or reflect those of the United States government or Lawrence Livermore National Security, LLC, and shall not be used for advertising or product endorsement purposes.

Density functional theory calculations of magnetocrystalline anisotropy energies for $(\text{Fe}_{1-x}\text{Co}_x)_2\text{B}$

Markus Däne¹, Soo Kyung Kim², Michael P. Surh¹, Daniel Åberg¹, and Lorin X. Benedict¹

¹ Lawrence Livermore National Laboratory, PO Box 808, L-372, Livermore, CA 94551, United States

² School of Materials Science and Engineering, Georgia Institute of Technology, Atlanta, 771 Ferst Dr. N.W. GA 30332-0245, United States

Abstract. We present and discuss density functional theory calculations of magnetic properties of the family of ferromagnetic compounds, $(\text{Fe}_{1-x}\text{Co}_x)_2\text{B}$, focusing specifically on the magnetocrystalline anisotropy energy (MAE). Using periodic supercells of various sizes (up to 96 atoms), it is shown that the general qualitative features of the composition dependence of the MAE is in agreement with experimental findings, while our predicted magnitudes are larger than those of experiment. We find that the use of small supercells (6 and 12-atom) favors larger MAE values relative to a statistical sample of configurations constructed with 96-atom supercells. The effect of lattice relaxations is shown to be small. Calculations of the Curie temperature for this alloy are also presented.

PACS numbers: 75.30.Gw, 71.70.Ej, 75.10.-b, 75.50.-y, 75.50.Ww, 03.65.-w

1. Introduction

There is currently an interest in searching for permanent magnet materials for electric motor applications that are alternatives to those in wide use which possess expensive Rare Earth (RE) elements such as Nb and Sm [1]. As various materials are explored for their potential applicability in this regard, important figures-of-merit include the energy product (related to the area enclosed by the magnetic hysteresis loop) and the Curie Temperature, T_C [2]. Only a material with a sizable energy product can perform useful work on its surroundings, and the temperature at which this work is performed must be comfortably below the temperature at which its total magnetic moment disappears. While T_C is largely a function of the size of the near-neighbor exchange energies, the energy product (closely related to the coercivity) is a multi-scale property which reflects the tendency of magnetic domains to resist reorientation when placed in an external field which is misaligned with them. This complex physics of domain wall structure, motion, and pinning is all dependent in part on a microscopic property:

the magnetocrystalline anisotropy energy (MAE), the energy required to reorient the electron spins in a ferromagnet from easy- to hard-axis directions [2, 3]. Though the energy product involves much more than the MAE, it is hard to imagine a material with a sizable energy product that does not also have a significant uniaxial MAE. Indeed, permanent magnets in wide industrial use, such as $\text{Sm}_2\text{Co}_{17}$ and $\text{Nd}_2\text{Fe}_{14}\text{B}$, possess fairly large MAEs [4] resulting from the interplay between the large spin-orbit interaction provided by the RE element together with the enhanced crystal field splitting in these tetragonal structures.

Rare Earth compounds are not the only ones to exhibit large MAE. For instance, CoPt, FePt [4], and the recently-studied Li_2FeN_5 [5] are just a few examples of materials with anisotropies which rival those of the permanent magnets in wide use. In general, the problem of searching for new reduced-RE permanent magnet alternatives should benefit from *ab initio* electronic structure calculations, from which T_C and MAE can be predicted. And in this case, Rare Earth compounds themselves present a formidable challenge, owing to the fact that they often possess narrow-band f -electron levels in the neighborhood of their Fermi energies, which are notoriously difficult to treat predictively. Various additions to density functional theory (DFT) such as DFT+U have been applied to the prediction of MAE in RE magnets [6, 7], but it is still unclear if such mean-field extensions are indeed suitably predictive for the purpose of designing new materials [8]. For CoPt and other such non-Rare Earth materials, however, the situation is thought to be slightly better with respect to *ab initio* calculations.

Recently, a team searching for Rare Earth-free permanent magnets suggested the compound $(\text{Fe}_{1-x}\text{Co}_x)_2\text{B}$ for $x \sim 0.3$ as a potential candidate [9]. They showed experimentally that both the coercivity and the MAE peak for the specific value $x \sim 0.3$, in agreement with earlier measurements from several decades before by Iga [10] and Takacs et al. [11]. This was quickly reconfirmed by another group of experimentalists [12], while Iga's higher- T results have been recently confirmed in Ref. [13]. In this latter work, a team involving coauthors of Ref.[9] studied the possibility of increasing the MAE further by alloying with other elements. Though the value of the MAE for the $(\text{Fe}_{0.7}\text{Co}_{0.3})_2\text{B}$ alloy is below that of some other candidate permanent magnets, several features of the $(\text{Fe}_{1-x}\text{Co}_x)_2\text{B}$ system are quite interesting from the perspectives of both applications and theory: 1. The T_C are reasonably high, and are known experimentally as a function of Co-concentration, x [11]. 2. The MAE is known not only as a function of x , but also as a function of temperature, T , throughout the full range of x [10, 11, 13]. 3. The crystal structure is thought to be essentially unchanged, modulo small changes in lattice parameters, throughout the full range of (x, T) [10]. 4. The electronic structure is devoid of partially occupied f -electron states. Point 4 bodes well for the application of first-principles electronic structure calculations of the DFT variety, while point 3 suggests that additional complications arising from structural complexity may not play a large role. Point 2 ensures that there is a wealth of data to which to compare, challenging the theoretical community to postdict both the detailed concentration- and temperature-dependence of the MAE, thereby providing a very useful testing ground

for current and developing strategies to predict this important quantity.

To this end, two very recent theoretical contributions have addressed the $(\text{Fe}_{1-x}\text{Co}_x)_2\text{B}$ system using DFT-based methods. The first [12], involving two co-authors of this manuscript and an experimental team mentioned above, proposed a detailed explanation of the composition-dependence of the MAE based on selection rules and band-filling arguments. First-principles calculations were performed in which the exchange-correlation \mathbf{B} -field was rescaled to produce agreement with the low- T magnetic moments throughout the full range of x (this required a single rescaling), and then the MAE as a function of x , calculated within the Coherent Potential Approximation (CPA) [14, 15, 16, 17, 18] to treat compositional disorder ($\text{Fe} \rightleftharpoons \text{Co}$), was shown to be in good agreement with low- T experimental data. The second [13], also involving the other team of experimentalists mentioned above, used the Virtual Crystal Approximation (VCA) to treat compositional variations together with a full-potential electronic structure approach to predict $\text{MAE}(x)$; they also noted the relationship between the sizes of the predicted moments and the overall magnitude of the MAE, and focused particularly on recommending strategies for further increasing the MAE on the Fe-rich side by doping.

The CPA and the VCA, while quite probably appropriate for predicting a range of properties for intermediate compositions in systems in which substitutional disorder is complete, do not allow for the investigation of the effects of detailed positional correlations on properties. This includes the spread in values that can occur if the disorder is in fact not complete, as well as the potential effects of local structural relaxations. Since the MAE in many materials is known to be very sensitive to crystal geometry, it is therefore also of interest to address such issues directly for the $(\text{Fe}_{1-x}\text{Co}_x)_2\text{B}$ system, as a complement to the aforementioned recent theoretical studies.

In this work, we perform *ab initio* electronic structure calculations of MAE, local spin moments, and T_C , as a function of Co-concentration for $(\text{Fe}_{1-x}\text{Co}_x)_2\text{B}$. For MAE and moments, we model the substitutional disorder for intermediate values of x with a set of discrete ordered supercells of different sizes, in which symmetrically inequivalent atomic orderings are considered. This allows us to examine the potential effects of local atomic positional relaxations, as well as the distribution of MAE and spin moment values for different substitutional arrangements of Fe and Co ions. The primary aims of this paper are three-fold: 1. To demonstrate that the general qualitative trends of the composition-dependent MAE for this system are described well by standard DFT, and that these qualitative features are relatively robust even when local substitutional disorder and resulting structural modifications are taken into account. 2. To confirm that the detailed magnitudes of the MAE are not described well by either LDA or GGA-DFT without additional corrections, such as those recently applied [12, 13]. 3. To show that the magnitudes of the MAE are further impacted by the detailed treatment of positional disorder, particularly on the Co-rich side. While we compare to experimental results throughout our work, we intentionally refrain from using the experimental magnetic moment and MAE values to guide the choices we make when performing our calculations. In this way, we intend to give the reader a picture of the

current state-of-the-art in the prediction of MAE using well-converged DFT calculations for a system exhibiting substitutional disorder.

The paper is organized as follows: In section 2, we provide computational details of the methods used as well as the details of our assumptions regarding the composition-dependent crystal structures. Curie temperatures are discussed in section 3. In Section 4, we show our results for the magnetocrystalline anisotropy energy as computed by DFT for different exchange-correlation functionals, including the role of lattice geometry, and compare to experiments [10, 11]. Our calculations of local spin moments are presented in Section 5, and their possible relation to the mis-prediction of the MAE is discussed. We summarize our findings and discuss potential future directions in Section 6.

2. Details of the calculations

Fe_2B and Co_2B have the same crystal structures, space group 140, $I4/mcm$, also known as the CuAl_2 prototype or C16. The boron atoms occupy the 4a $(0,0,1/4)$ positions, and the iron or cobalt atoms the 8h $(\xi, 1/2+\xi, 0)$ sites. Experimental values for ξ are 0.1661 for Fe_2B and 0.1663 for Co_2B [10]. The crystal structure is shown in Figure 1. For intermediate concentrations, we assume the crystal structure to be the same. This is compatible with the limited x-ray diffraction studies performed on this suite of materials for intermediate x [10], and the efficacy of this assumption will be further strengthened when our results for T_C are compared to those of experiment.

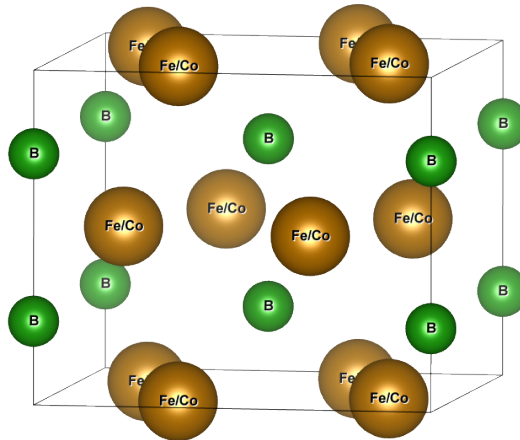


Figure 1. $(\text{Fe/Co})_2\text{B}$ cell (Al_2Cu prototype (C16)), spacegroup 140, $I4/mcm$. B occupies the 4a $(0,0,1/4)$ Wyckoff positions, Fe and Co the 8h $(\xi, 1/2+\xi, 0)$ with $\xi=0.1661(\text{Fe}_2\text{B})$ and $\xi=0.1663(\text{Co}_2\text{B})$.

Since MAE values in particular are expected to be somewhat sensitive to atomic positions, the bulk of our DFT calculations of these quantities are performed with lattice parameters which are inferred from x-ray diffraction measurements on Fe_2B and Co_2B at various temperatures, together with a limited number of diffraction measurements

performed on $(\text{Fe}_{1-x}\text{Co}_x)_2\text{B}$ for $x = 0.6$ [10]. Since we are ultimately interested in examining the MAE throughout the full range of x (and the appropriate values of T to make proper comparisons with experiment), we fit a model for the three C16 crystal structure parameters: tetragonal cell lengths a and c , and internal parameter ξ to fix the unit cell geometry for any given (x, T) . Our fits to the experimental data for a and c are shown in Fig. 2, and the fits are of the form:

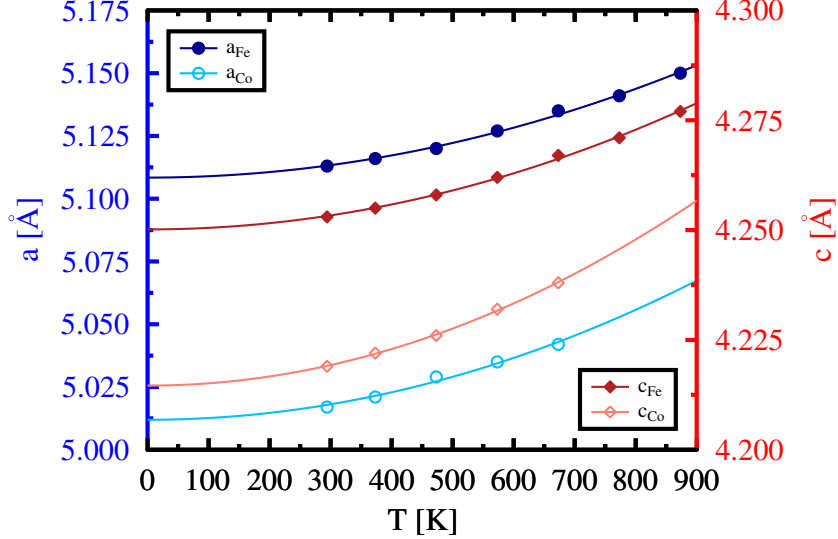


Figure 2. Lattice parameters for Fe_2B and Co_2B as a function of T . The experimental values [10] appear as dots, and our fits to these data are represented by the curves.

$$\begin{aligned}
 a_{\text{Fe}}(T) &= 5.10841 + (5.52348 \times 10^{-8}) T^2 \\
 c_{\text{Fe}}(T) &= 4.25016 + (3.54608 \times 10^{-8}) T^2 \\
 a_{\text{Co}}(T) &= 5.01195 + (6.84340 \times 10^{-8}) T^2 \\
 c_{\text{Co}}(T) &= 4.21460 + (5.19616 \times 10^{-8}) T^2 \\
 a(x, T) &= (1 - x)[a_{\text{Fe}}(T)] + x[a_{\text{Co}}(T)] \\
 c(x, T) &= (1 - x)[c_{\text{Fe}}(T)] + x[c_{\text{Co}}(T)] \\
 \xi(x) &= (1 - x)[0.1661] + x[0.1663],
 \end{aligned} \tag{1}$$

where the subscripts "Fe" and "Co" indicate lattice constants for Fe_2B and Co_2B , T is in Kelvin, and a and c are in Å. The fits for a_{Fe} , c_{Fe} , a_{Co} , and c_{Co} are constructed solely from the T -dependent data of Ref. [10] pertaining to Fe_2B and Co_2B ; the lattice constants for the intermediate Co-concentrations are *assumed* to depend on them in the manner given above, which is a reasonable first assumption in the absence of a large collection of additional data. The one additional set of data for the single value $x = 0.6$ [10] shows our fit for $a(x = 0.6, T = 293\text{K})$ to be too low by 0.14% and our fit for

$c(x = 0.6, T = 293\text{K})$ to be too high by 0.2%. We will see below that the consequence of these discrepancies on the value of the predicted MAE is negligible. We assume that the internal parameter, ξ , of the intermediate-concentration cases linearly interpolates between its measured values for Fe_2B ($\xi = 0.1661$) and Co_2B ($\xi = 0.1663$). No appreciable variation of this parameter with temperature was mentioned in conjunction with the x-ray measurements [10]. Our results below show only a very small dependence of the MAE on the choice of ξ within its reasonable range of variation.

For our calculations of MAE values, we use the VASP plane wave DFT code [19, 20, 21, 22] with projector augmented wave (PAW) pseudopotentials [23, 24]. The non-collinear spin-density functional (Pauli equation) formalism is used [25]. Unless otherwise specified, we employ the generalized gradient approximation (GGA) within the PBE scheme [26]. We also make comparisons where appropriate to results obtained using the local density approximation (LDA). Plane wave cutoffs and energy convergence criteria for the determination of the self-consistent charge density are chosen very conservatively, given the PAWs for these elements, to ensure that the MAE is computed to the maximum precision consistent with the method. As discussed at length by many authors (see for instance Ref. [3] and references therein), the MAE is highly sensitive to both the number of \mathbf{k} -points used in Brillouin zone (BZ) integrations, and the energy broadening (or \mathbf{k} -space interpolation scheme) employed. We use 21^3 , 17^3 , and 5^3 Γ -centered \mathbf{k} -point meshes for the 6, 12, and 96 atom-cell MAE calculations, respectively. These calculations are sped up by making use of crystal symmetry operations to reduce the \mathbf{k} -points to an irreducible wedge, which in the presence of spin-orbit is a relatively recent addition to VASP [27]. Both tetrahedral interpolation [28] and Gaussian broadening schemes are used for the representations of the sums of occupied Kohn-Sham eigenvalues in the computations of the total energies; very limited dependences of the MAE with respect to these choices are observed, given the \mathbf{k} -point mesh sizes we employ. We use two different schemes to compute the MAE: (i) The self-consistent method, in which total energies for different spin polarization directions, E_{\parallel} and E_{\perp} , are computed independently by calculating separate charge densities in the presence of the spin-orbit term, ρ_{\parallel} and ρ_{\perp} . (ii) The non self-consistent method, in which the charge density (determined in calculations neglecting spin-orbit) for each spin polarization are presumed to be equal, and E_{\parallel} and E_{\perp} are each determined by adding spin-orbit as a perturbation in which Kohn-Sham eigenvalues are converged in its presence, but ρ is not updated. As expected from the relative smallness of the spin-orbit term (which results in small MAEs, generally), these two methods produce essentially identical results for the systems we study here.

For our calculations of T_C for various Co-concentrations, we use the Korringa-Kohn-Rostoker (KKR) [29, 30] DFT code, Hutsepot, within the coherent potential approximation (CPA) [14, 15, 16, 17, 18, 31, 32]. This allows us to obtain Heisenberg exchange energies [33] J_{ij} from which we calculate T_C from a standard Monte-Carlo

algorithm. All such KKR calculations, to obtain the effective J_{ij} parameters, are performed within the collinear spin density functional formalism (using PBE), in which no spin-orbit interaction is considered. We find that including the interactions with the nearest 1000 neighboring sites is sufficient to converge the Monte Carlo calculations with the Heisenberg Hamiltonians. T_C is then determined by identifying the peak in the T -dependent heat capacity for each concentration.

Our use of two separate DFT codes, VASP (plane-wave, pseudopotential) and Hutsepot (KKR-ASA) is motivated by the following several points: 1. The multiple-scattering formalism adopted in the Greens function KKR method makes the calculation of exchange parameters (J_{ij}) needed for the determination of T_C very straightforward. 2. This KKR-ASA code is also equipped with the means to do alloy calculations within the CPA, which we employ below for both for the calculation of composition-dependent J_{ij} and magnetic moments. The use of CPA is not possible within VASP; comparisons of local moment calculations with VASP using super-cells and Hutsepot using CPA are informative, as discussed in Section 5. 3. VASP with the appropriate PAW potentials is effectively full-potential, while ASA is not, and we deem it important to use full-potential calculations wherever possible when predicting the MAE, since this quantity is known to be quite sensitive to details of the total energy calculations. 4. VASP is equipped with accurate forces and sophisticated geometrical relaxation schemes that enable the lattice relaxation studies we report here.

3. Calculations of T_C

Figure 3 displays our results (dashed red curve) along with those of experiment [11] (blue points). The agreement is excellent, though notable deviations can be seen for small x . Still, this level of agreement indicates that our assumptions regarding the absence of major x -dependent structural modifications are probably correct, since significant (x, T) -dependent modifications to the crystal structure of the real system would likely result in larger changes to $T_C(x)$ (it is noteworthy that the elemental Fe and Co systems in their native lattices have $T_C[\text{Fe}] < T_C[\text{Co}]$, in contrast to that shown here and in Ref.[11] for Fe_2B and Co_2B). While this result for the Curie temperature is somewhat decoupled from those that follow, it is at least encouraging that this important property is described well by PBE for the assumed C16 structure with complete Fe \leftrightarrow Co substitutional disorder as modeled by the CPA.

4. Calculations of magnetocrystalline anisotropy energies

For the purpose of calculating the MAE for different Co-concentrations, x , we model $(\text{Fe}_{1-x}\text{Co}_x)_2\text{B}$ with a set of discrete ordered structures. This is certainly approximate, but it does allow us to estimate the magnitudes that local relaxations of the atomic positions might have on the MAE. We first use a 12 atom (8Fe/Co + 4B) cell, allowing for concentrations $x = 0, 0.125, 0.25, 0.375, 0.5, 0.625, 0.75, 0.875, \text{ and } 1.0$. Figure 1

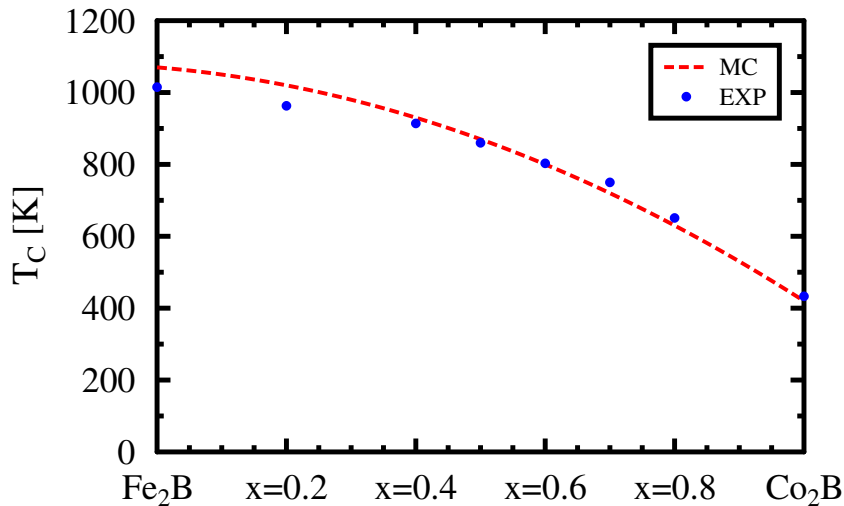


Figure 3. (color online) Curie temperatures, T_C , versus Co-concentration for the $(\text{Fe}_{1-x}\text{Co}_x)_2\text{B}$ system. Experimental data [11] are indicated by blue dots. Red dashed curve shows the results of our PBE calculation of exchange parameters using KKR-ASA, together with a determination of T_C using a Monte Carlo (MC) approach as applied to the resulting Heisenberg Hamiltonian, in which 1000 nearest-neighbor couplings are used.

illustrates the 12-atom C16 structure cell, in which alternating planes of B and Fe/Co are seen. For each concentration, we compute the MAE for all possible symmetrically inequivalent arrangements of Fe/Co atoms. In addition, the MAE at zero temperature ($= E_{\perp} - E_{\parallel}$) is computed by considering two mutually orthogonal spin-polarization directions in the (\perp) plane. In this way, we obtain a spread of MAE values for each x .

Figure 4 shows four distinct sets of MAE results using the 12-atom cells. Upper panels indicate calculations performed with the lattice parameters from the fit of Eq. 1 with $T = 0$, using LDA (upper left) and PBE (upper right) as the exchange correlation functional. Individual MAE values for particular ordered configurations of Fe and Co, and for particular choices of planar spin polarization direction, appear as blue dots. The red curves connect MAE results for which the particular 12-atom configurations have the lowest predicted total energies. Within this cell representation of $(\text{Fe}_{1-x}\text{Co}_x)_2\text{B}$, the red curve is the $T = 0$ prediction. The orange curve connects MAE values averaged with weights determined from Boltzmann factors involving the total energies of the particular ionic configurations, and evaluated for $T = 293\text{K}$ (even though the lattice geometry parameters, $\text{MAE}(\nu)$, and E_{ν} are chosen to be those meant for $T = 0$):

$$\text{MAE}(T) \equiv \sum_{\nu} [\text{MAE}(\nu) \exp(-E_{\nu}/k_{\text{B}}T)] / \sum_{\nu} \exp(-E_{\nu}/k_{\text{B}}T), \quad (2)$$

where E_{ν} denotes the total energy of atomic arrangement ν . Shaded regions indicate the spread in these values (standard deviation). Taken together, these upper panel figures show several features: LDA and PBE predictions of $\text{MAE}(x)$ are generally similar, with the exception of the endpoints, $x = 0$ and $x = 1$, exhibiting changes of sign. Other

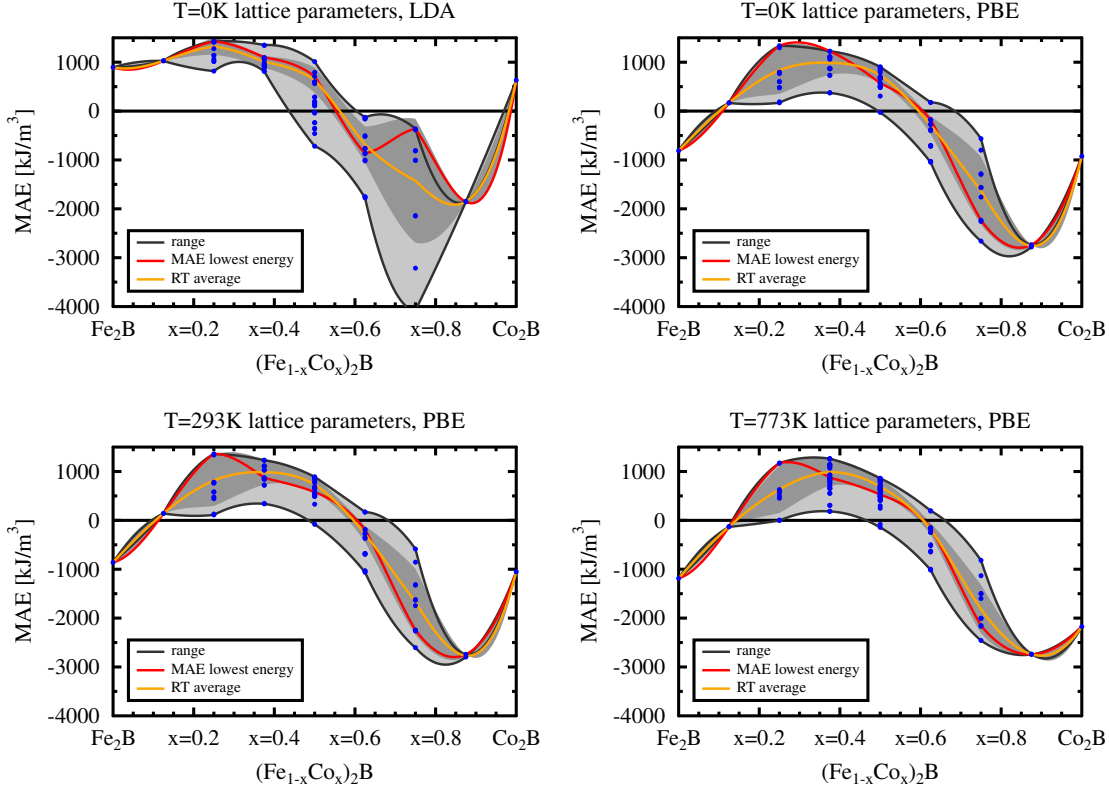


Figure 4. (color online) DFT predictions of MAE for discrete structures using a 12 atom cell. The temperatures listed at the top of each figure correspond to the experimentally-derived lattice parameters used [10]; all MAE results are constructed by differencing total energies computed at $T = 0$. The light shaded area marks the range of obtained anisotropies (blue dots), where the red curve connects those which are lowest in total energy. The yellow line corresponds to a room temperature average of anisotropies, the standard deviation is shown by the dark shaded areas.

than this, $\text{MAE}(x) \equiv E_{\perp} - E_{\parallel}$ is positive (indicating an easy axis along \mathbf{c}) for lower Co-concentrations, and is negative (planar easy axis) for higher Co-concentrations. This is in broad agreement with experiment [9, 10], though our predicted magnitudes of the MAE are considerably larger than the measured values. We replot the experimental results of Ref. [10] in Fig. 5 using the same scale and axes as those of Fig. 4; in Fig. 5, red symbols indicate the spread of values for a given x measured from $T = 77$ to $T \sim 800$ K, and the blue curve connects MAE values measured at $T = 77$ K [10]. Note that our predicted MAE (for PBE and especially LDA) exhibit a particularly large spread for $x = 0.75$ for these 12-atom periodic cells, and that the largest values of MAE for this concentration are more than four times larger in absolute value than those of experiment. The two bottom panels of Fig. 4 are just like the PBE plot in the upper right, but with lattice parameters chosen from the fits of Eq. 1 for $T = 293\text{K}$ and $T = 773\text{K}$, respectively. The minute differences between the three PBE panels of Fig. 4 indicate a very small dependence of the calculated $\text{MAE}(x)$ on the measured T -dependent variations in lattice parameters, for which the underlying lattice is assumed

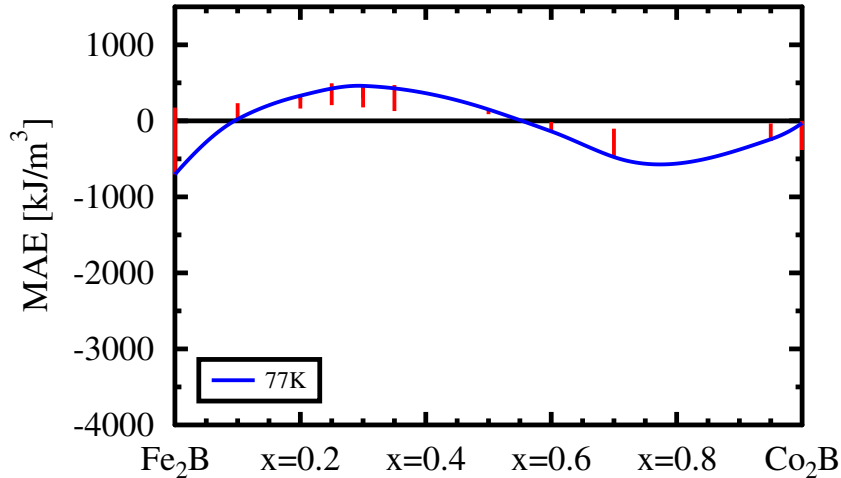


Figure 5. (color online) Experimental MAE values taken from Ref. [10] (red points) at each Co-concentration; data from all temperatures are overlaid. The blue curve goes through the MAE values measured at $T = 77$ K.

to be ideal and of the C16 type.

It is noteworthy that the upper-right panel of Fig. 4 is very similar to the analogous predictions shown in Fig. 6 of Ref. [13], obtained using the VCA. Indeed, the only notable deviation when comparing their results to, say, our red curve, is the slightly smaller value of x at which the MAE attains its maximum (our ~ 0.3 vs. their ~ 0.4). As we will see below, however, the magnitudes of the MAE, particularly for Co-rich cases, reduce in absolute value when the supercell size is increased.

Turning briefly to the nature of the dependence of the total energy on spin polarization direction, Fig. 6 shows the MAE defined as $E_\theta - E_\parallel$ calculated (in the non self-consistent mode) with PBE for Fe_2B and Co_2B as a function of the angle θ , which is defined as angle of the spin polarization direction to the c -axis. $\theta = 90^\circ$ represents spin polarization directions along a planar direction. The lattice parameters from the $T = 0$ fit for $x = 0, 1$ are used, as in the upper right panel of Fig. 4. We see from Fig. 6 that PBE predicts Fe_2B to be a uniaxial magnet, for which there is a clear easy axis (i.e., no multiple minima). Our calculations for structures with intermediate- x display essentially identical behavior, indicating that DFT predicts uniaxial anisotropy in this system, as is desired for permanent magnet applications. We also find the anisotropy in plane to be extremely small for both Fe_2B and Co_2B , suggesting that the choice of planar direction in the computation of E_\perp is largely immaterial. For intermediate- x discrete structures, this is less so; our computation of E_\perp for orthogonal planar directions contributes to the spreads in MAE values for given intermediate x values as shown in Fig. 4.

4.1. lattice relaxations

One advantage of using discrete ordered structures is that it allows us to study the possible effects of local atomic arrangements on the MAE. Since it is generally the case

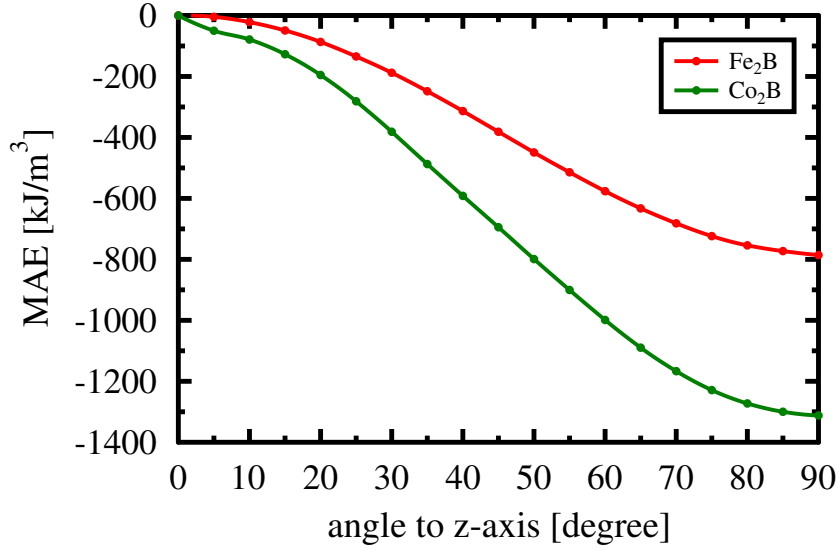


Figure 6. (color online) PBE predictions of the MAE as a function of spin polarization direction (90 degrees indicating the planar direction) for Fe_2B and Co_2B .

that GGA is slightly more reliable for geometry optimization than LDA, we use PBE to relax the various structures with VASP's geometry optimization capability. For these we use periodically repeated 6 atom cells ($4\text{Fe}/\text{Co}+2\text{B}$). First we study the equilibrium cell volumes one obtains for $(\text{Fe}_{1-x}\text{Co}_x)_2\text{B}$, keeping internal coordinates fixed. Figure 7 shows (PBE) relaxed cell volumes as a function of Co-concentration for (red crosses). These predictions lie below those obtained by our fits (lines, generated from Eqs. 1) to

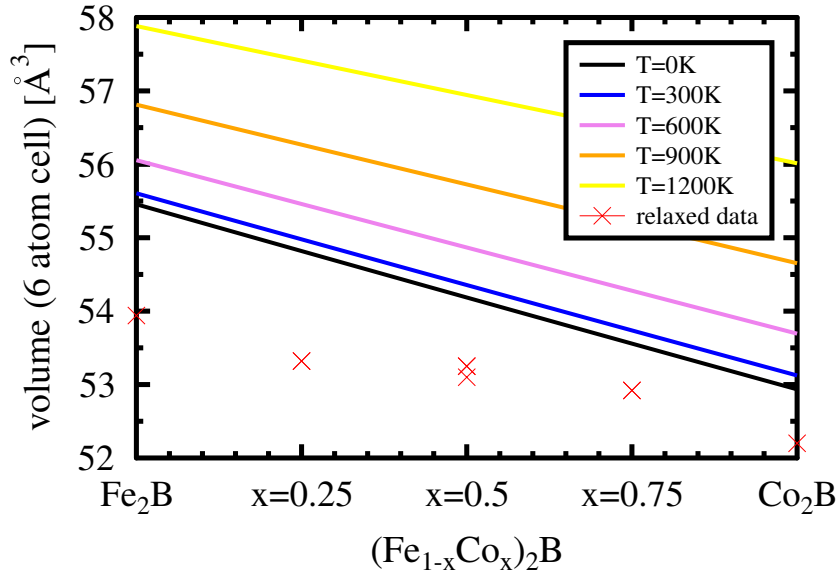


Figure 7. (color online) Relaxed cell volumes computed with PBE for the 6 atom cells (red crosses). Curves indicate the cell volumes as determined from the experimentally-derived fits; the black curve is the (extrapolated) fit result for $T=0$.

experiment [10] by up to $\sim 2.5\%$.

Next we investigate how structural relaxations affect the anisotropies. Figure 8 shows our results for relaxed and unrelaxed cases using both LDA and PBE. As with

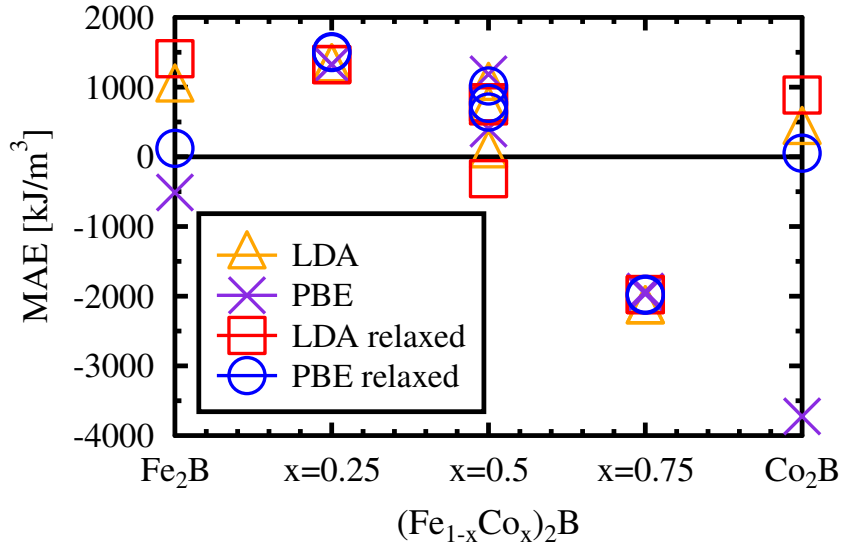


Figure 8. (color online) DFT predictions of MAE for discrete structures using a 6 atom cell performed with both relaxed and unrelaxed atomic geometries. See text for details.

the 12-atom cells, we display results for all symmetrically inequivalent configurations, though here we refrain from considering each inequivalent polarization direction in the computations of E_{\perp} . Four types of results are displayed: Orange triangles (LDA) and purple crosses (PBE) show the MAE calculated with the experimentally determined room- T lattice geometry of Fe_2B (irrespective of x). Red squares (LDA) and blue circles (PBE) show the MAE calculated at lattice geometries determined for each cell individually by relaxing internal atomic positions (as well as cell volume and shape) using PBE. The LDA vs. PBE comparison shows sign flips for $x = 0$ and $x = 1$, as we saw for the 12-atom cases. The effect of relaxing the atomic positions is largest for $x = 0, 1$ as well, and is particularly dramatic for the PBE calculation of the MAE of Co_2B . However, the overall shape of $\text{MAE}(x)$ is again similar to that of the 12-atom cell results (see Fig. 4), and it is even the case that assuming a single structure (that of Fe_2B ; orange triangles and purple crosses) produces results which are broadly similar to those assuming the more detailed concentration-dependent structures implied by Eqs. 1. We note that the insensitivity of the $x = 0.25$ and $x = 0.75$ cases to both changes in exchange-correlation functional and to atomic relaxation is quite striking. This suggests that the $x = 0.3$ case discussed recently in Ref. [9] may be more robustly described here, though we stress once again that the magnitude of the MAE is overpredicted (compare to Fig. 5) relative to experiment in the standard DFT treatments we employ.

We also explore the dependence of the anisotropy of the pure systems, Fe_2B and Co_2B , on the C16 internal parameter, ξ , which is also not perfectly reproduced in PBE

relaxations. In these calculations, we choose the lattice parameters a and c from Eq. 1 for $T = 0$. Figure 9 shows the dependence of both the MAE and the total energy on ξ . Our results (top panel) indicate that the optimal value of ξ within PBE is ~ 0.1670 rather than the 0.1661-0.1663 seen in experiment [10]. However, the bottom panel shows that

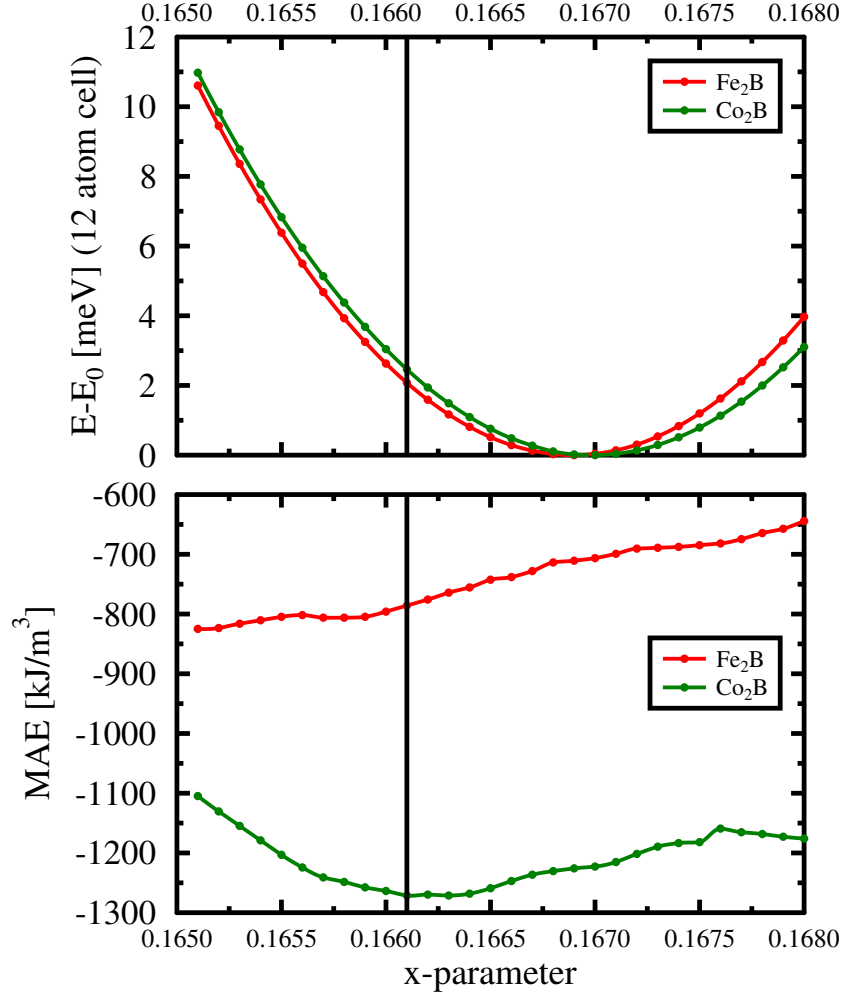


Figure 9. (color online) PBE predictions for the dependence of the MAE on the internal parameter, ξ , based on the experimentally-derived $T=0$ a and c lattice parameters for Fe_2B and Co_2B (lower panel). The upper picture shows the total energy versus ξ . The experimental value of $x = 0.1661$ (for Fe_2B) is marked by a vertical line.

the computed effect of this particular discrepancy on the MAE is modest on the scale of the variations seen in Fig. 4. Thus, the fact that this internal parameter is slightly off from what it should be is not likely to be the cause of the MAE theory-experiment discrepancy we see here.

4.2. 96-atom supercells

We have noted a sizable spread in our predicted MAE values using all possible configurations for a given concentration within a 12-atom cell. We have also seen that the bulk of these MAE values are substantially larger in absolute value than those found in experiment. This prompts us to consider even larger supercells, in order to investigate if the use of small cells biases the results in a particular direction. To this end, we choose 96 atom cells, in which VASP calculations are performed as before, but with a 5^3 \mathbf{k} -point mesh. We first note that even with this moderately sparse sampling of the Brillouin zone we are able to reproduce the MAE of periodic repetitions (12PR) of the configurations studied for the 12-atom cell with a 21^3 \mathbf{k} -point mesh, see Fig. 10 (compare red and orange points). Since the large number of configurations makes it

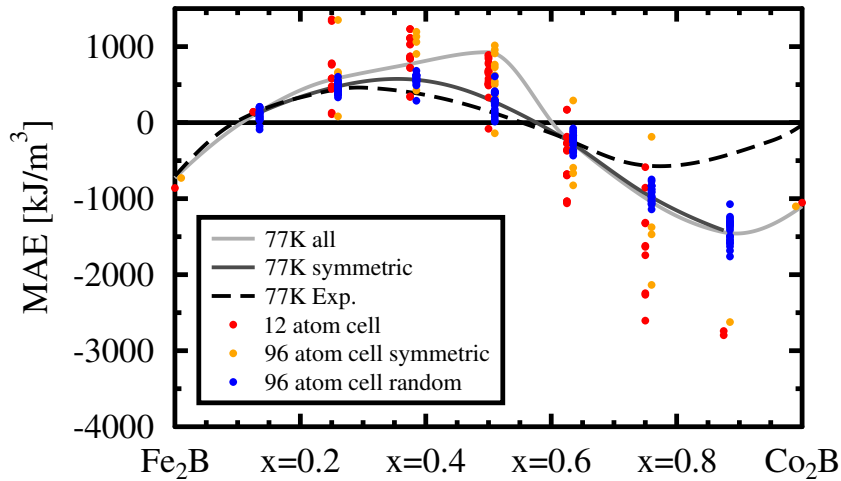


Figure 10. (color online) comparison of MAE (PBE) data obtained with a 12-atom cell (red dots) and a 96-atom (orange and blue, data points are slightly shifted horizontally) cell. The label 'symmetric' refers to configurations which can be realized in a 12-atom cell, where 'random' indicates a random distribution of Fe and Co atoms within the cell, corresponding to a certain concentration. The dashed black line marks the experimental 77K data of Iga et. al. [10]. The two solid lines are the 77K by Boltzmann factors weighted averages (see Eq. 2), including all 'symmetric' and 'random' configurations as well as 'random' configurations only.

unfeasible for us to calculate the MAE of every possible periodic cell of this size, we limit ourselves to at most twenty representative random configurations per concentration. The resulting *limited* distribution of MAEs (Fig. 10) from this set (96PR, blue points) curiously display less spread than those of the 12PR configurations. Furthermore, the absolute magnitudes of the MAE of this set are in general *smaller* than those from the 12PR set, and particularly so for the Co-rich cases in the neighborhood of $x \sim 0.8$. We note that the $x = 0.875$ 12PR case contains a chain of Fe atoms and has a positive enthalpy of formation as predicted by PBE, highlighting the problematic nature of using the smaller super cells for modeling the effect of disorder on the MAE. At this point it is again instructive to study the temperature dependent Boltzmann-weighted MAEs

defined in Eq. 2. Figure 10 contains a comparison between experimental and predicted (with and without the 12PR structures) MAE at 77 K. Since the 12PR structures are over-represented in this limited average, it is perhaps more reasonable to consider the thermodynamic average *excluding* this set as more accurate. With this approximation – as well as those of the underlying exchange correlation functional – in mind, we see the averages of the random configurations using larger supercells better match experiment than those of the highly periodic 12 atom supercells. This suggests that a treatment of true disorder could produce better agreement still; the use of the CPA in the calculation of MAE values for this system has been investigated in a recent work [12].

4.3. temperature effects

Since the T -dependence of $\text{MAE}(x)$ has been measured for $(\text{Fe}_{1-x}\text{Co}_x)_2\text{B}$ [10], it is of interest to know how much of this detailed T -dependence, if any, can be obtained in the calculations by simply performing $T = 0$ electronic structure calculations of the MAE at the T -dependent experimental lattice parameters, as for example suggested in reference [34]. We have already seen from Fig. 4 that the variation of the computed $\text{MAE}(x)$ with different lattice parameters is minimal.

Figure 11 (left panel) shows our MAE calculated (12 atom cells) with PBE for Fe_2B and Co_2B using the experimentally-derived T -dependent lattice parameters of Eq. 1, and plotted against T . For comparison (right panel) are the T -dependent MAE

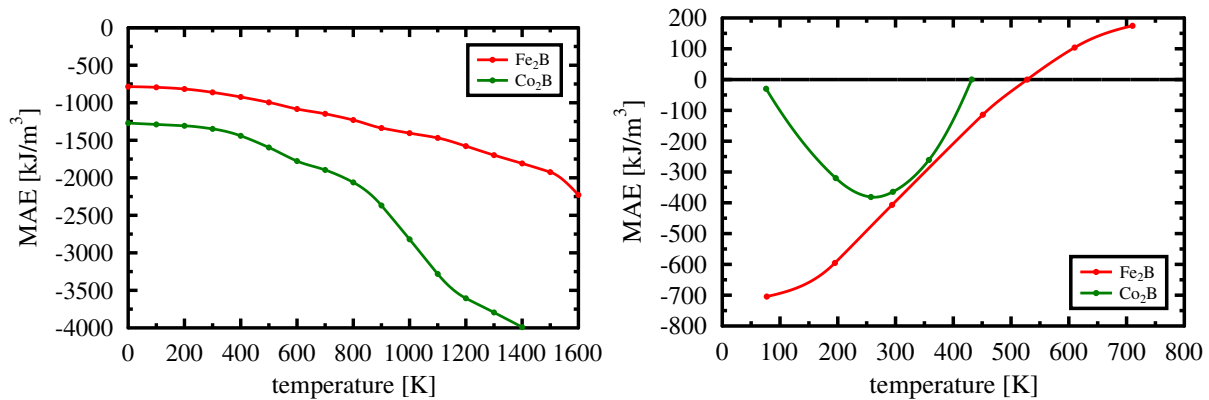


Figure 11. (color online) left: Calculated ($T = 0$) MAE (PBE), computed at the experimental lattice parameters [10] for different temperatures for Fe_2B and Co_2B . right: experiment, data from Ref. [10]

from experiment [10]. It is clear that even the qualitative trends in the predictions are incorrect; the anisotropy for Fe_2B decreases (i.e., becomes more negative) rather than increasing, and the anisotropy of Co_2B decreases monotonically, in contrast to the non-monotonic behavior seen in experiment. This suggests that an inclusion of spin-disorder, rather than simple thermal expansion, is necessary to describe much of the T -dependence of the MAE in this system, even well below the Curie temperature. This important subject awaits further study.

5. Calculations of magnetic moments

Our LDA and PBE results for the MAE are larger in magnitude than those of experiment, even when considering the larger super cells possessing an ostensibly better description of disorder (compare the blue curves/symbols of Figs. 5 and 10). Given that the experiment-theory discrepancy for MAE is particularly large on the Co rich side, it is natural to study the composition-dependence of more basic magnetic properties, namely the magnetic moments, and to compare them to the available experimental results, as also explored in recent works [12, 13]. Figure 12 shows KKR-CPA total moments for the range of concentrations (black solid curve) compared with those from the measurements of Takacs et al. [11] (blue dots). While the predictions within PBE agree with the experimental results for the Fe-rich compounds, they lie well above those of experiment on the Co-rich side, and progressively more so for larger x . The general reduction of total moment with increasing x is easily understood from band-filling arguments. However, our calculations also suggest that the Fe moment (not weighted by concentration), per Fe ion, is nearly constant for different x while the Co moment, per Co ion, decreases by nearly $0.2\mu_B$ as x increases from 0 to 1. That is illustrated by the solid red (Fe) and green (Co) curves in Fig. 12. A change in the Co

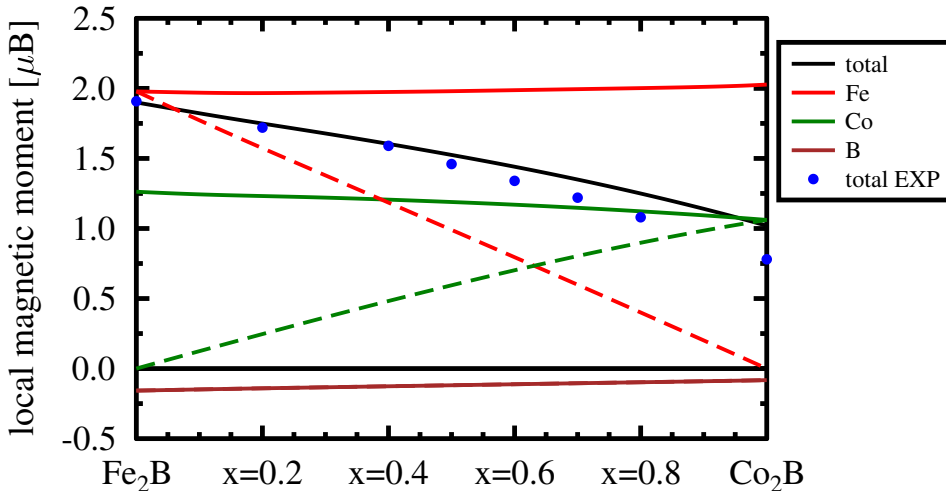


Figure 12. (color online) Calculated (continuous curves) using KKR-CPA and estimated magnetic moments from experiment [11] (blue dots). Solid lines show the local moments on each lattice site based on a CPA calculation. Dashed lines shows the moments weighted by their concentrations.

moment with increasing Co-concentration was also suggested in conjunction with the experimental findings [11], though again it seems that our reduction with x is not as large as that of experiment. The concentration-weighted individual contributions to the total moment appear as dashed curves. The B moments are predicted to be extremely small and anti-ferromagnetically aligned with the Fe/Co (brown curve). While these results confirm those of Refs.[12, 13], it is important to note that the same trends can be

observed from VASP calculations using discrete structures as discussed above, shown in Figure 13. Solid lines are those of CPA-KKR calculations (same as in Figure 12), dots

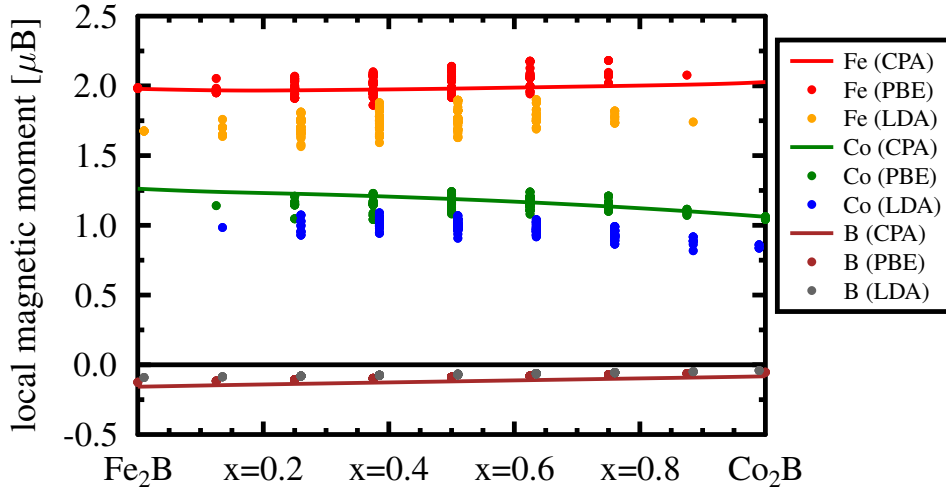


Figure 13. (color online) Calculated local magnetic moments (dots) using all possible discrete supercells in a 12 atom cell, for LDA and PBE. Solid lines show KKR-CPA PBE data for comparison.

correspond to magnetic moments of all 12-atom configurations computed with VASP. The magnitudes and distributions of moments from the 96-atom cells are very similar. The PBE KKR-CPA moments are in good agreement with the VASP calculations using the discrete structures, even though there is a significant spread indicating that changes in local environment give rise to changes in moments. The main point is that the moments calculated with PBE are significantly larger than those of experiment for the same values of x for which our predicted MAE are similarly too large. This is consistent with the observations made in Refs.[12, 13] and in [34] for a different material, which further argued the need to ensure that local moments are predicted accurately before an accurate MAE can be computed.

It is interesting to note that the LDA total moment for Co_2B (blue dot on the RHS of Fig. 13) is not much larger than that inferred from experiment (blue dot on the RHS of Fig. 12), and yet our LDA prediction of the MAE of Co_2B is still quite a bit larger in absolute value than that of experiment (though with a sign-flip relative to the PBE prediction; see Figs. 4 and 5). It is however true that the LDA values of MAE for $x = 0.75$ and 0.875 are notably smaller, on average, than those of PBE (compare upper left and upper right panels of Fig. 4), which coincides with the fact that both Fe and Co moments are substantially smaller in LDA. As we noted above, however, the $x = 0.25$ MAE does not show a substantial variation, LDA vs. PBE, and it is even the case that the average value of the spread in the upper-right panel (PBE) of Fig. 13 is lower than that in the upper-left panel (LDA). This seems to contradict the aforementioned correlation between moment size and MAE magnitude, since the LDA moments are quite a bit lower than the PBE moments throughout the

full range of x shown in Fig. 13, including $x = 0.25$. It suffices to say that the correct prediction of moments is certainly not a sufficient condition for the accurate prediction of MAE. Further detailed analysis of both 12-atom and 96-atom results reveals no correlation between the spatial distributions and overall sizes of moments for given ionic configurations and the computed MAE for the same configurations.

As we mentioned in the Introduction, DFT + U methods have been used to predict magnetic properties of RE compounds, where f-electron localization is clearly relevant. Since standard DFT of the PBE-GGA variety seems to give incorrect moments for Co in the $(\text{Fe}_{1-x}\text{Co}_x)_2\text{B}$ system, it is worth asking if the application of a correlation correction of this type for the Co d-electron manifold might lead to results in better agreement with experiment. Though we stated at the outset that our aim in this work is to refrain from using experimental moment data to guide our choices, we note that such an inclusion does not automatically lead to improved agreement here: Applying a $U - J$ (using the so-called rotationally invariant formalism of Dudarev et al. [35]) to the Co-d states increases the (PBE-GGA) Co spin moments for Co_2B , pushing them farther from the experimental results. In particular, $U - J = 1$ eV gives a μ_{Co} roughly 20% higher than the $U - J = 0$ value shown as the left-most solid green line in Fig. 12, while the experimental value for μ_{Co} is $\sim 20\%$ lower.

In recent works concerning the MAE of both this system [12, 13] and others [34], the correlation between the under(over)-prediction of local spin moments, and a corresponding under(over) prediction of the MAE was emphasized. In Ref. [12] for $(\text{Fe}_{1-x}\text{Co}_x)_2\text{B}$, a rescaling of the exchange-correlation \mathbf{B} -field on the Co ions was applied to reduce the Co-moment to a value in line with experiment, and the resulting MAE (as computed with an LMTO-ASA approach using the CPA with the PBE functional) was then also shown to fall in line with the experimental values [10]. Given that this rescaling prescription 1. is questionable, in that it does not arise from a consistent theoretical description, and 2. is merely *postdictive* as it relies on input from experiment, we submit that the further studies along these lines are needed.

6. Conclusions

We have investigated the magnetic properties of the $(\text{Fe}_{1-x}\text{Co}_x)_2\text{B}$ system using Density Functional Theory. We conclude that Curie temperatures can be determined reasonably well over the whole concentration range by performing Monte-Carlo simulations with Heisenberg exchange parameters determined from DFT. The basic qualitative shape of the dependence of the MAE on the Co concentration is similar to that of experiment, even though our predicted magnitudes are too large, depending on the treatment of disorder. We note that better agreement is obtained for larger supercells. However we show that both LDA and PBE support the proposal [9] that an alloy with $x \sim 0.3$ should be a good candidate for a uniaxial permanent magnet. We also find the calculated MAE to be relatively insensitive to finer details of the atomic geometry, including local positional relaxations and the precise value of the internal parameter ξ . Calculations of

the MAE using T -dependent lattice parameters ($a(T, x)$ and $c(T, x)$) along with zero- T ferromagnetic ground states failed to predict even the qualitative trends in the measured T -dependent MAE, suggesting that other effects, such as thermal spin fluctuations even well below T_C , phonon-magnon coupling, or effects of magnetorestriction may need to be considered. It was demonstrated that the MAE of the ordered structures, Fe_2B and Co_2B , depends strongly on the choice of the exchange correlation functional, exhibiting sign-flips, while the intermediate- x cases are less affected by this choice.

The incorrect predictions of the total moments in both LDA and PBE variants of DFT for this system are troubling, and may indeed be another important cause for incorrectly predicted MAE values at low- T , as suggested in recent works [12, 13]. It will therefore be important in the future to explore different strategies for improving DFT in a consistent manner so that such *ab initio* calculations of MAE are truly predictive. This, together with the inclusion of thermally-induced disorder to model the highly-detailed T -dependent features of the MAE of $(\text{Fe}_{1-x}\text{Co}_x)_2\text{B}$, are likely to be fruitful areas for future work.

Acknowledgments

We thank Babak Sadigh for many helpful suggestions. This work was supported by the Laboratory Directed Research and Development (LDRD) Program at LLNL under tracking code No. 13-ERD-044, and the Critical Materials Institute (CMI), an Energy Innovation Hub funded by the U.S. Department of Energy. T_c and 96-atom supercell MAE calculations were performed under the LDRD, and 12-atom supercell MAE calculations were performed within the CMI. Investigations of the local spin moments were performed under both LDRD (VASP calculations), and CMI (KKR-ASA calculations). This work was performed under the auspices of the U.S. Department of Energy by Lawrence Livermore National Laboratory under Contract DE-AC52-07NA27344.

References

- [1] Coey J 2002 *Journal of Magnetism and Magnetic Materials* **248** 441–456 ISSN 0304-8853 URL <http://www.sciencedirect.com/science/article/pii/S0304885302003359>
- [2] Coey J 2009 *Magnetism and Magnetic Materials* (Cambridge University Press) ISBN 978-0521816144
- [3] Jansen H 1991 Magnetic anisotropy *Science and Technology of Nanostructured Magnetic Materials* (NATO ASI Series vol 259) ed Hadjipanayis G and Prinz G (Springer US) pp 349–365 ISBN 978-1-4899-2592-3 URL http://dx.doi.org/10.1007/978-1-4899-2590-9_40
- [4] Skomski R 2003 *Journal of Physics: Condensed Matter* **15** R841 URL <http://stacks.iop.org/0953-8984/15/i=20/a=202>
- [5] Antropov V P and Antonov V N 2014 *Phys. Rev. B* **90**(9) 094406 URL <http://link.aps.org/doi/10.1103/PhysRevB.90.094406>
- [6] Larson P, Mazin I I and Papaconstantopoulos D A 2003 *Phys. Rev. B* **67**(21) 214405 URL <http://link.aps.org/doi/10.1103/PhysRevB.67.214405>

- [7] Steinbeck L, Richter M and Eschrig H 2001 *Phys. Rev. B* **63**(18) 184431 URL <http://link.aps.org/doi/10.1103/PhysRevB.63.184431>
- [8] Bousquet E and Spaldin N 2010 *Phys. Rev. B* **82**(22) 220402 URL <http://link.aps.org/doi/10.1103/PhysRevB.82.220402>
- [9] Kuzmin M D, Skokov K P, Jian H, Radulov I and Gutfleisch O 2014 *Journal of Physics: Condensed Matter* **26** 064205 URL <http://stacks.iop.org/0953-8984/26/i=6/a=064205>
- [10] Iga A 1970 *Japanese Journal of Applied Physics* **9** 415 URL <http://stacks.iop.org/1347-4065/9/i=4/a=415>
- [11] Takacs L, Cadeville M C and Vincze I 1975 *Journal of Physics F: Metal Physics* **5** 800 URL <http://stacks.iop.org/0305-4608/5/i=4/a=021>
- [12] Belashchenko K D, Ke L, Däne M, Benedict L X, Lamichhane T N, Taufour V, Jesche A, Bud'ko S L, Canfield P C and Antropov V P 2015 *Applied Physics Letters* **106** 062408 (*Preprint* [1501.03483](https://arxiv.org/abs/1501.03483))
- [13] Edström A, Werwiński M, Rusz J, Eriksson O, Skokov K P, Radulov I A, Ener S, Kuz'min M D, Hong J, Fries M, Karpenkov D Y, Gutfleisch O, Toson P and Fidler J 2015 *ArXiv e-prints* (*Preprint* [1502.05916](https://arxiv.org/abs/1502.05916))
- [14] Soven P 1967 *Phys. Rev.* **156**(3) 809–813 URL <http://link.aps.org/doi/10.1103/PhysRev.156.809>
- [15] Taylor D W 1967 *Phys. Rev.* **156**(3) 1017–1029 URL <http://link.aps.org/doi/10.1103/PhysRev.156.1017>
- [16] Winter H and Stocks G M 1983 *Phys. Rev. B* **27**(2) 882–904 URL <http://link.aps.org/doi/10.1103/PhysRevB.27.882>
- [17] Johnson D D, Nicholson D M, Pinski F J, Györffy B L and Stocks G M 1986 *Phys. Rev. Lett.* **56**(19) 2088–2091 URL <http://link.aps.org/doi/10.1103/PhysRevLett.56.2088>
- [18] Johnson D D, Nicholson D M, Pinski F J, Györffy B L and Stocks G M 1990 *Phys. Rev. B* **41**(14) 9701–9716 URL <http://link.aps.org/doi/10.1103/PhysRevB.41.9701>
- [19] Kresse G and Hafner J 1993 *Phys. Rev. B* **47**(1) 558–561 URL <http://link.aps.org/doi/10.1103/PhysRevB.47.558>
- [20] Kresse G and Hafner J 1994 *Phys. Rev. B* **49**(20) 14251–14269 URL <http://link.aps.org/doi/10.1103/PhysRevB.49.14251>
- [21] Kresse G and Furthmüller J 1996 *Phys. Rev. B* **54**(16) 11169–11186 URL <http://link.aps.org/doi/10.1103/PhysRevB.54.11169>
- [22] Kresse G and Furthmüller J 1996 *Computational Materials Science* **6** 15 – 50 ISSN 0927-0256 URL <http://www.sciencedirect.com/science/article/pii/0927025696000080>
- [23] Blöchl P E 1994 *Phys. Rev. B* **50** 17953–17979
- [24] Kresse G and Joubert D 1999 *Phys. Rev. B* **59**(3) 1758–1775 URL <http://link.aps.org/doi/10.1103/PhysRevB.59.1758>
- [25] Hobbs D, Kresse G and Hafner J 2000 *Phys. Rev. B* **62**(17) 11556–11570 URL <http://link.aps.org/doi/10.1103/PhysRevB.62.11556>
- [26] Perdew J P, Burke K and Ernzerhof M 1996 *Phys. Rev. B* **77** 3865–3868 erratum, *ibid.* **78**, 1396(E) (1997)
- [27] Åberg D, Sadigh B and Erhart P 2012 *Phys. Rev. B* **85**(12) 125134 URL <http://link.aps.org/doi/10.1103/PhysRevB.85.125134>
- [28] Blöchl P E, Jepsen O and Andersen O K 1994 *Phys. Rev. B* **49**(23) 16223–16233 URL <http://link.aps.org/doi/10.1103/PhysRevB.49.16223>
- [29] Korringa J 1947 *Physica* **13** 392 – 400 ISSN 0031-8914 URL <http://www.sciencedirect.com/science/article/pii/003189144790013X>
- [30] Kohn W and Rostoker N 1954 *Phys. Rev.* **94**(5) 1111–1120 URL <http://link.aps.org/doi/10.1103/PhysRev.94.1111>
- [31] Györffy B and Stocks G 1979 First principles band theory for random metallic alloys *Electrons in Disordered Metals and at Metallic Surfaces* (NATO Advanced Study Institutes Series vol 42) ed

- Phariseau P, Györffy B and Scheire L (Springer US) pp 89–192 ISBN 978-1-4684-3502-3 URL http://dx.doi.org/10.1007/978-1-4684-3500-9_4
- [32] Györffy B, Johnson D, Pinski F, Nicholson D and Stocks G 1989 The electronic structure and the state of compositional order in metallic alloys *Alloy Phase Stability (NATO ASI Series vol 163)* ed Stocks G and Gonis A (Springer Netherlands) pp 421–468 ISBN 978-94-010-6901-4 URL http://dx.doi.org/10.1007/978-94-009-0915-1_28
- [33] Liechtenstein A, Katsnelson M, Antropov V and Gubanov V 1987 *Journal of Magnetism and Magnetic Materials* **67** 65–74 ISSN 0304-8853 URL <http://www.sciencedirect.com/science/article/pii/0304885387907219>
- [34] Antropov V P, Antonov V N, Bekenov L V, Kutepov A and Kotliar G 2014 *Phys. Rev. B* **90**(5) 054404 URL <http://link.aps.org/doi/10.1103/PhysRevB.90.054404>
- [35] Dudarev S L, Botton G A, Savrasov S Y, Humphreys C J and Sutton A P 1998 *Phys. Rev. B* **57**(3) 1505–1509 URL <http://link.aps.org/doi/10.1103/PhysRevB.57.1505>